Proceedings of the 2000 Winter Simulation Conference
J. A. Joines, R. R. Barton, K. Kang, and P. A. Fishwick, eds.

TIRE MODEL FOR SIMULATIONS OF VEHICLE MOTION ON HIGH AND LOW FRICTION ROAD SURFACES

James Lacombe

U.S. Army Engineer Research and Development Center (ERDC)
Cold Regions Research and Engineering Laboratory (CRREL)
72 Lyme Road
Hanover, NH 03755-1290, U.S.A.

ABSTRACT

An on-road analytical tire model has been developed to predict tire forces and moments at the tire/road interface. The model is computationally efficient and it only requires a limited set of easily obtained input parameters. Force and moment calculations are based on mechanical analogs that describe longitudinal and lateral tire tread and sidewall deflections during braking, traction and cornering. Longitudinal deflections are determined using a simple linear elastic spring model, while lateral deflections are calculated using an elastic beam model. Surface sliding friction is defined by experimental curves relating the friction coefficient to the wheel/road differential velocity. Source code has been developed to include the model as a force element subroutine in commercially available dynamic analysis software known as DADS (Dynamic Analysis Design System). The tire model has been successfully demonstrated in DADS using a simple simulation of a tire test device. Preliminary comparisons of model predictions with available test data have been favorable. Efforts are underway to incorporate the tire subroutine into a DADS model of a HMMWV to conduct driving simulations on dry, snow and ice covered road surfaces.

1 INTRODUCTION

On-road vehicle mobility is important to the military, as it is a major factor governing the movement of troops and materiel in the field. Accurate representations of wheeled vehicle maneuvering capabilities (traction, braking and cornering) are needed via high-resolution dynamic simulations to predict maximum over-the-road vehicle speeds as road conditions worsen due to degraded weather. Several commercial software products exist for creating such simulations, one being DADS (Dynamic Analysis Design System, LMS CAE, Coralville, Iowa). Personnel at the Cold Regions Research and Engineering Laboratory (CRREL) are using DADS to create dynamic simulations of vehicles operating under winter conditions.

A critical element in any wheeled vehicle dynamic model is the set of algorithms that defines the interaction between tire and road. A model is provided in the current version of DADS (Version 9.5) that predicts tire response to vertical loading. It is used here, and is discussed in more detail later in the paper. A tire model is also provided in DADS that predicts longitudinal and lateral reaction forces and moments during combined traction (or braking) and cornering. This is the so-called Magic model by Pacejka and Bakker (1993).

The Magic model is empirical, requiring specification of a number of parameters determined from experimental measurements of tire forces and moments. Such measurements require sophisticated test equipment however, which makes the Magic model impractical for organizations with modest tire-testing capabilities. Also, the Magic model is not well suited to parametric studies of the impacts of snow and ice induced changes in surface friction on vehicle performance. A static friction coefficient appears in the model, but it determines peak forces and moments only. Its adjustment alone does not properly account for the variation in surface friction commonly observed at different tire/road slip conditions. A full compliment of force and moment measurements seems to be required instead for each road surface condition examined. Hence, an alternative tire model is needed that: 1) only requires a limited set of easily measured tire input parameters, 2) is analytical in nature, with physically meaningful parameters that directly relate to tire characteristics and road surface conditions, 3) realistically accounts for changes in surface friction and 4) is numerically simple and practical for use in complex vehicle simulations. A steady-state form of solution is adequate since the problem being addressed is low-frequency vehicle maneuvering on smooth non-deformable road surfaces.

2 TIRE MODEL DEVELOPMENT

Numerous approaches to tire modeling are documented in the literature. Two simple ones are adopted here to describe tire deflections and forces in the vertical (i.e., normal to the road surface) and longitudinal (in the tire plane, tangent to the road surface) directions. A novel approach involving elastic beam theory is used to define displacements and forces in the third "lateral" direction.

2.1 Force and Moment Conventions

Figure 1 shows the force and moment vectors calculated by the tire model being discussed. These act at the central intersection point of the tire disk and road surface plane. They constitute an equivalent orthogonal representation of the road forces generated along the displaced tire patch. The x and z axes shown are parallel to the longitudinal axis of the tire and the road surface normal, respectively.

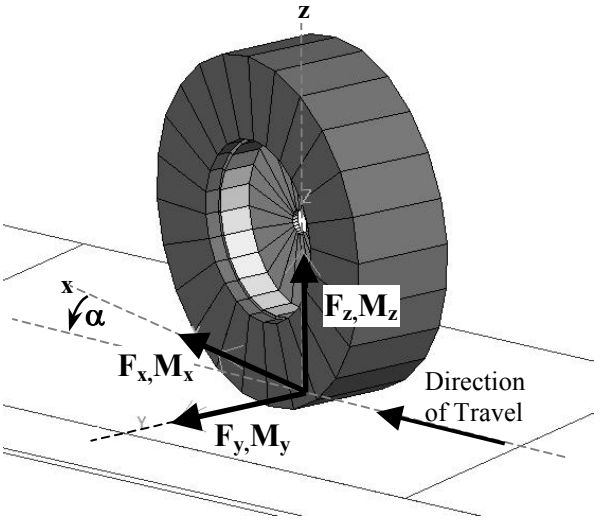

Figure 1: Calculated Tire Forces and Moments

2.2 Vertical Tire Response

"Vertical" tire/road interactions (i.e., normal to the road surface along the z axis) are treated independently of lateral and longitudinal interactions, and calculated using the *distributed contact model* currently in DADS. This model describes tire normal deflections and velocities based on the lateral cross-sectional area generated by an equivalent undeformed disk intersecting with the road profile. The normal deflection of the actual flattened tire is computed from the intersected arc length of the undeformed disk. Tire normal force is calculated using a simple linear spring model with user-specified spring constant. The latter is easy to measure; Table 1 lists the spring constant K_{vert} for a light-truck tire that was determined from measurements made at CRREL.

Damping can be affected as well in the normal direction in the current DADS code if the user provides a damping constant. The stiffness and damping constants can also be replaced by empirically-based curves. A complete description of the distributed contact model is provided in Chapter 12.16 of the DADS Reference Manual.

2.3 Longitudinal Tire Response

Longitudinal tire/road interactions are represented in the CRREL tire model by a simple 1-dimensional quasi-static "Brush" (or "Cantilevered Spoke") mechanical analog described by Dixon (1996) and a nominal expression for rolling resistance. Figure 2 depicts the Brush analog.

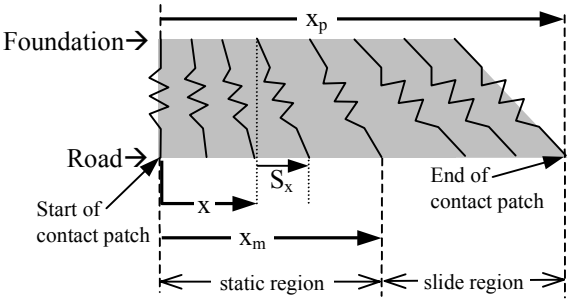

Figure 2: "Brush" Analog used to Describe Longitudinal Tire Behavior alongTire Contact Patch

2.3.1 Tire Patch Static Region

In the Brush model, the contact patch is divided into two sections: a forward "static" region where the tire tread adheres to the road surface, and an aft "slide" region where sliding occurs between tire and road. Contact patch displacement is limited by the tire longitudinal foundation stiffness C_l and surface frictional forces. In the forward static region, at a distance x from the leading edge of the patch, the tire tread stretches an amount S_x equal to:

$$S_x = \left(1 - \frac{V_x}{\omega R}\right) x \tag{1}$$

where V_x is the velocity of the wheel center in the longitudinal direction, ω is the wheel rotation rate and R is the tire rolling radius. The longitudinal friction force $f_{x,st}$ exerted on the tire in the static region is the product of S_x and the foundation stiffness C_l, integrated from x = 0 to x_m, where x_m marks the transition point from the static to sliding regions. This equates to:

$$f_{x,st} = \frac{C_l}{2}\left(1 - \frac{V_x}{\omega R}\right) x_m^2 \tag{2}$$

The tire foundation stiffness C_l can be obtained from a simple static pull test. Figure 3 shows the test setup used at CRREL to determine C_l. A load cell capable of measuring horizontal and vertical forces supports a vertically loaded tire. The load cell itself is supported by a frictionless bearing, which is pulled by a pneumatic cylinder. Longitudinal load and tire displacement are recorded and plotted, and the slope of the resulting curve determined. This value is then divided by the length of the tire contact patch to arrive at the foundation stiffness. A value for C_l for a light truck tire is included in Table 1.

Figure 3: CRREL Test Apparatus for Measuring Tire Foundation Stiffness

2.3.2 Tire Patch Slide Region

Sliding friction generates the longitudinal forces that act against the aft "slide" region of the tire patch. To simplify calculation of these forces, the following assumptions are made within the model.

The normal contact pressure along the entire length of the tire patch is treated as a constant. Its value is F_z/x_p, with F_z calculated in the manner described in Section 2.2. x_p is estimated to be some fraction of the maximum dimension observed in tire contact area data, since contact pressure is known to peak near the center of the contact patch and diminish asymptotically at the leading and trailing edges. At the present time, x_p is estimated to be one half the maximum patch dimension (x_{max}) documented from inked tire print measurements; i.e., $x_p/x_{max}= ½$. Note that an approximation of a fixed value for x_p ignores "stretching" in the static region of the tire patch, which is implied by the brush model in Figure 2. This is done to simplify the computation of tire patch lateral deflections. Fore and aft stretching of the tire patch is accounted for in the calculation of aligning moments however, as it is here that the effects of stretching are likely to have the greatest impact.

x_{max} (inches) is related to normal load F_z (lbs.) by the following empirical equation.

$$x_{max} = \left[\frac{4F_z}{m_{est}} \left(2R_u - F_z / m_{est} \right) \right]^{1/2} \tag{3}$$

R_u (inches) is the undeflected tire radius and m_{est} (lbs/in) is an empirically determined patch length coefficient.

Another assumption made in the model is that the tire tread sliding friction properties are isotropic. This permits a non-directional sliding friction coefficient "μ" to be used to define the net sliding friction force vector $f_{xy,sl}$ acting opposite to the direction of tire *sliding motion*. The magnitude of this force equals the product of μ and the normal force acting in the slide region, i.e.:

$$f_{xy,sl} = \mu \frac{F_z \left(x_p - x_m \right)}{x_p} \tag{4}$$

It then follows that the sliding lateral and longitudinal forces combine according to a "friction circle" (or friction ellipse), as discussed by Gillespie (1992), with a limiting force defined by Equation 4. The sliding friction force generated in either the longitudinal or lateral direction equals $f_{xy,sl}$ multiplied by the ratio of the x or y and net sliding velocities. The sliding velocities in the x and y directions are $\omega R\text{-}V_x$ and $V_x*\mathrm{Tan}(\alpha)$, respectively, with α being the tire slip angle shown in Figure 1. For the longitudinal direction, the sliding friction force $f_{x,sl}$ equals:

$$f_{x,sl} = \left[\frac{\omega R - V_x}{\left(V_x^2 \mathrm{Tan}^2(\alpha) + (\omega R - V_x)^2 \right)^{1/2}} \right] \frac{\mu F_z \left(x_p - x_m \right)}{x_p}$$

or

$$f_{x,sl} = \frac{\left(\omega R / V_x - 1 \right) \mu F_z \left(x_p - x_m \right)}{\left(\mathrm{Tan}^2(\alpha) + (\omega R / V_x - 1)^2 \right)^{1/2} x_p} \tag{5}$$

Similarly, the lateral sliding friction force $f_{y,sl}$ equals:

$$f_{y,sl} = \frac{\mathrm{Tan}(\alpha) \mu F_z \left(x_p - x_m \right)}{\left(\mathrm{Tan}^2(\alpha) + (\omega R / V_x - 1)^2 \right)^{1/2} x_p} \tag{6}$$

The sliding friction coefficient μ is defined as a function of the net sliding velocity in the x-y plane. This is similar to the practice of reporting tire friction coefficient as a function of either DIV (differential interface velocity, i.e., ωR - vehicle speed) or "slip" (ωR/vehicle speed – 1). Curves based on the former are utilized in the model since

"slip", as defined, has no meaning in the lateral direction. Figure 4 provides examples of how sliding friction is represented in the model. The dry pavement curve is generated from St. Germann, Wurtenberger and Daib (1994) and the snow curve from Shoop (1993). Only those sections of the cited authors' curves corresponding to pure sliding have been transposed. Friction coefficients shown in Figure 4 for low sliding velocities (where both stiction and sliding are evident in the original DIV curves) are extrapolated estimates that are much higher than the values in the original curves at the same differential velocities (represented by the dashed curves). The friction coefficient rises as velocity drops, reaching a maximum at, essentially, the static condition, as discussed by Ichihara (1971) and Yamazaki, Furukawa and Suzuki (1997). The friction coefficient is estimated using a stepwise linear approximation to the friction curve.

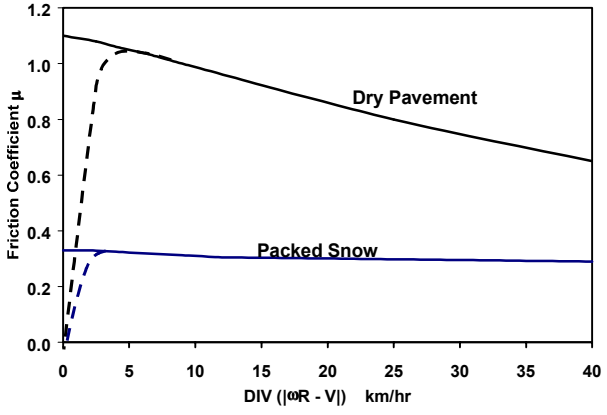

Figure 4: Sample Curves - Sliding Friction Coefficient

2.3.3 Rolling Resistance

The rolling resistance force F_{rr} is estimated to be some small fraction k_{rr} (typically 1-5 %) of the tire normal force; i.e.,

$$F_{rr} = -k_{rr} F_z \tag{7}$$

Rolling resistance acts in the longitudinal direction only.

2.3.4 Net Longitudinal Force

The net longitudinal force is the sum of Equations 2, 5 and 7. This results in the following solution for F_x.

$$F_x = \frac{C_l}{2}\left(1 - \frac{V_x}{\omega R}\right)x_m^2 + \frac{\left(\omega R / V_x - 1\right)\mu F_z \left(x_p - x_m\right)}{\left(\mathrm{Tan}^2(\alpha) + \left(\omega R / V_x - 1\right)^2\right)^{1/2} x_p} - k_{rr} F_z \tag{8}$$

2.4 Lateral Tire Response

Lateral tire behavior is non-linear and complex, and most often described using empirical and semi-empirical approaches (Pacejka and Bakker (1993), Brach and Brach (2000) and Nicholas and Comstock (1972)). In addition, several analytical models exist, such as the one described by Shim, Margolis and Belltawn (2000). This model simulates combined braking and cornering, but is limited to linear tire behavior at small slip angles. Ellis (1969) proposes two analytical models for tire lateral response: the taut string with elastic curtain and the beam on an elastic foundation. While the former, like the previously discussed model, is only applicable to small slip angles, the latter applies to all longitudinal and lateral slip conditions. The mathematical derivation for Ellis' elastic beam model uses several numerical approximations however, and he treats tread and carcass/sidewall deflections separately. Application of the model, either by its author or others, is not evident in the literature as well. The beam-on-elastic-foundation is a useful analog nonetheless, and an alternate set of equations is offered here to describe it.

2.4.1 Elastic Beam Theory

The tire is treated as a beam restrained by an elastic foundation attached to a fixed base (wheel rim). Beam deflection represents tire tread lateral deflection, which follows a linear path in the static region of the tire patch determined by the slip angle α, and a parabolic curve in the slide region (Figure 5).

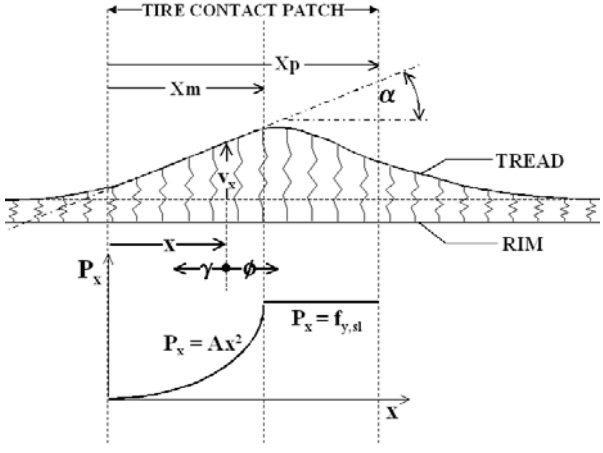

Figure 5: Plan View of Tire Patch Lateral Deflection using a Beam on Elastic Foundation Model

2.4.1.1 Lateral Tire Deflection

Using classic elastic beam theory (Timenshenko 1960), tire patch deflection is calculated according to:

$$v_x = \int_0^{x_p - x} \frac{P_x \beta}{2k} e^{-\beta\phi}\left(\cos(\beta\phi) - \sin(\beta\phi)\right)d\phi + \int_0^{x} \frac{P_x \beta}{2k} e^{-\beta\gamma}\left(\cos(\beta\gamma) - \sin(\beta\gamma)\right)d\gamma \quad (9)$$

where P_x is the lateral shear stress due to tire/road friction at some distance x from the leading edge of the tire contact patch, k is the foundation stiffness modulus, v_x is the lateral tire patch deflection at x, and ϕ and γ are displacements from x as shown in Figure 5. β is defined as:

$$\beta = \sqrt[4]{\frac{k}{4EI}} \quad (10)$$

The product of E (Modulus of Elasticity) and I (Moment of Inertia) is referred to as the beam Flexural Rigidity (Popov 1967).

P_x is calculated in one of two ways, depending on whether x falls in the static or slide region of the tire patch (i.e., $0 \le x \le x_m$ or $x_m < x \le x_p$). A functional form is assumed for P_x in the static region. This is necessary for a solution to Equation 9 to be possible. A simple linear function is avoided, as the rise in lateral static friction is intuitively expected to be non-linear. A parabolic function (Equation 11) is used instead.

$$P_x = Ax^2 \quad (\text{for } 0 \le x \le x_m) \quad (11)$$

where the coefficient "A" is determined for each tire "state". An exponential function was also examined, but it resulted in deflection and force predictions that were very close to the values reached using the parabolic function, suggesting that the form of non-linear equation used is not critical. For the slide region, P_x equals $f_{y,sl}$ (Equation 6) divided by $(x_p - x_m)$.

Equation 9 evaluates to two solutions for v_x, again depending on whether $x \le x_m$ or $x > x_m$.

$$v_x = f_1\{x, x_m, x_p, A, f_{y,sl}, \beta, k\} \quad \text{for } x \le x_m \quad (12)$$

$$v_x = f_2\{x, x_m, x_p, A, f_{y,sl}, \beta, k\} \quad \text{for } x > x_m \quad (13)$$

"A" is determined by evaluating Equation 12 at x=0 and $x=x_m$, and equating the difference to the product of x_m and $\tan(\alpha)$; i.e.,

$$v_{x=x_m} - v_{x=0} = x_m \tan(\alpha) \quad (14)$$

with Equation 14 leading to:

$$A = f_3\{x_m, x_p, f_{y,sl}, \beta, k, \alpha\} \quad (15)$$

The detailed solutions to Equations 12, 13 and 15 are listed in Appendix A.

2.4.2 Estimating k and β

The foundation stiffness "k" and the coefficient "β" are determined using the same elastic beam analysis applied to the moving tire. In this instance however, it is applied to a stationary tire subjected to a static lateral load. Lateral tire stiffness K_{lat} is documented by loading the tire in the manner shown in Figure 6. This is identical to the arrangement described in Section 2.3.1, except that the tire is pulled laterally instead of longitudinally. The lateral force on the tire is not allowed to exceed a value that causes it to slide against the load plate supporting it. The slope of the force-displacement curve generated defines K_{lat}.

Figure 6: CRREL Test Apparatus for Measuring Tire Lateral Stiffness

For the static tire case, lateral deflections along the entire contact patch are assumed to be equal (with zero slope). Applying appropriate boundary conditions, the deflection of an equivalent beam on an elastic foundation is defined as:

$$v_x = ce^{-\beta x}\left(\cos(\beta x) + \sin(\beta x)\right) \quad (16)$$

where x is the distance measured from the edge of the contact patch (or "$x + x_p/2$" from the centerline of the tire).

β, k and the coefficient "c" are related by the following equations:

$$\beta = \frac{2}{K_{lat}/k - x_p} \quad \text{and} \quad c = \frac{F_t}{k\left(x_p + 2/\beta\right)} \tag{17}$$

where F_t is the lateral force applied to the tire. Values for k and β are estimated by first noting the approximate distance (from the center of the contact patch) that the lateral deflection reaches zero, and then iteratively solving Equations 16 and 17 for different values of k until the predicted zero deflection (i.e., the *x* at which v_x is ~zero) agrees with observation. Figure 7 shows this methodology applied to a light truck tire; 36 psi appears to be a reasonable estimate for k. This leads to a solution for β of 0.148 in^{-1}.

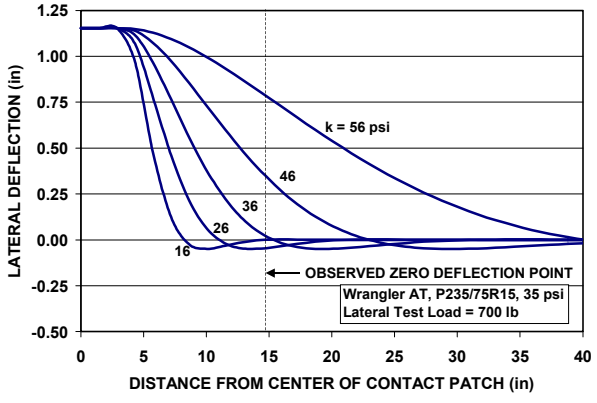

Figure 7: Tread Deflection Predictions for a Static Laterally Loaded Tire

2.4.3 Calculating x_m

The correct solution for the length of the tire patch static region x_m is the largest value, ≤ x_p, for which: 1) the net friction shear stress does not exceed the maximum possible static friction stress and 2) the slope of the lateral deflection matches the tangent of the slip angle α. The process for solving x_m is necessarily an iterative one. Requirement Number 1 is mathematically represented by:

$$\left(Ax_m^2\right)^2 + \left(C_1\left(1 - \frac{V_x}{\omega R}\right)x_m\right)^2 \le \left(\frac{\mu_o F_z}{x_m x_p}\right)^2 \tag{18}$$

μ_o is the friction coefficient from the tire/road friction curve at zero DIV (Figure 4.). Requirement Number 2 is defined by an error tolerance that quantifies how much the solution for the lateral deflection is permitted to diverge from the desired straight line in the static region of the tire patch. This error tolerance "ε" is represented by Equation 19, which computes the fractional error for the predicted lateral displacement halfway between the leading edge of the tire patch and the static/slide transition point. The error itself results from the fact that Equation 11 is an *estimate* for the shape of the lateral stress distribution in the static region.

$$\left|\frac{v_{x_m/2} - \left(v_{x=0} + \frac{x_m}{2}\tan(\alpha)\right)}{v_{x=0} + \frac{x_m}{2}\tan(\alpha)}\right| < \varepsilon \tag{19}$$

$v_{x=0}$ and $v_{x_m/2}$ represent the predicted lateral displacements (from Equation 12) for the leading edge of the tire patch and the position halfway between the leading edge and the static/slide transition point.

2.4.4 Net Lateral Force

The net lateral force (F_y) equals the lateral stress P_x integrated over the length of the entire contact patch. This results in the following solution for F_y.

$$F_y = \frac{A}{3}x_m^3 + \frac{\mathrm{Tan}(\alpha)\mu F_z\left(x_p - x_m\right)}{\left(\mathrm{Tan}^2(\alpha) + \left(\omega R / V_x - 1\right)^2\right)^{1/2} x_p} \tag{20}$$

2.5 Roll and Aligning Moments

The model also calculates the tire Roll moment (M_x) and the Aligning moment (M_z). The former results from the action of road surface normal forces about moment arms generated by the lateral deflection of the tire patch. M_x is represented as:

$$M_x = \int_0^{x_p} \frac{F_z}{x_p} v_x \, dx \tag{21}$$

As previously discussed, the solution for lateral deflection v_x varies depending on whether x is less than or greater than x_m. This results in Equation 21 being expressed as:

$$\begin{aligned} M_x = {} & \frac{F_z}{x_p}\int_0^{x_m} f_1\left\{x, x_m, x_p, A, f_{y,sl}, \beta, k\right\}dx \\ & + \frac{F_z}{x_p}\int_{x_m}^{x_p} f_2\left\{x, x_m, x_p, A, f_{y,sl}, \beta, k\right\}dx \end{aligned} \tag{22}$$

or

$$M_x = f_3\left\{x, x_m, x_p, A, F_z, f_{y,sl}, \beta, k\right\} \tag{23}$$

The aligning moment M_z results from: 1) lateral forces acting relative to the center of the tire patch, 2) longitudinal forces acting at the moment arms generated by tire patch lateral deflection and 3) lateral forces acting at the moment arms generated by tire patch longitudinal deflection. These effects are represented by:

$$M_z = \int_0^{x_m} Ax^2\left(x - \frac{x_p}{2}\right)dx + \int_{x_m}^{x_p} \frac{f_{y,sl}}{x_p - x_m}\left(x - \frac{x_p}{2}\right)dx + \int_0^{x_m} C_l S_x v_x dx + \int_{x_m}^{x_p} \frac{f_{x,sl}}{x_p - x_m} v_x dx \qquad (24)$$

$$- \int_0^{x_m} Ax^2 S_x dx - \int_{x_m}^{x_p} \left(\frac{f_{y,sl}}{x_p - x_m}\right)\frac{f_{x,sl}}{C_l\left(x_p - x_m\right)}dx$$

or

$$M_z = f_4\left\{x, x_m, x_p, S_x, C_l, A, F_z, f_{x,sl}, f_{y,sl}, \beta, k\right\} \qquad (25)$$

Detailed solutions to Equations 23 and 25 are listed in Appendix B.

3 MODEL IMPLEMENTATION IN DADS

The tire subroutine source code in DADS has been modified to incorporate the tire model described in Section 2. A simple simulation of a tire tester device was created and used to debug and fully implement the new code in DADS. The tire tester is shown in Figure 8. In this simulation, a tire supports a dead weight while being guided along a ramp at constant speed and constant slip angle. Longitudinal slip is gradually varied during the simulation such that the tire is free rolling at the beginning and fully braked by the end.

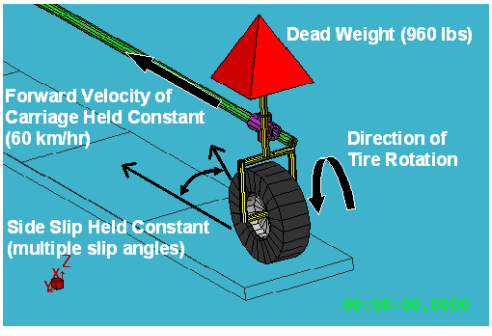

Figure 8: DADS Tire Tester Simulation

3.1 Tire Force and Moment Predictions

Figures 9-14 display sample predictions of tire forces and moments for different slip angles from the tire tester simulation. The tire-input parameters used are those listed in Table 1.

Table 1: Tire Model Parameters for a Light Truck Tire

Goodyear Wrangler AT, P235/75R15, 35 psi

Vertical Stiffness	K_{vert} = 1327 lb/in
Longitudinal Foundation Stiffness	C_l = 284 lb/in^2
Lateral Foundation Stiffness	k = 36 lb/in^2
Rolling Resistance Coefficient	k_{rr} = 0.01
$\beta = \sqrt[4]{\frac{k}{EI}}$	β = 0.148 in^{-1}
Undeflected Tire Radius	R_u = 14.438 in
Patch Length Coefficient	m_{est} = 2300 lb/in

Figures 9 and 10 show longitudinal and lateral forces generated during combined cornering and braking on dry pavement for all ranges of longitudinal slip (i.e., braking) and slip angles of 2 and 5 degrees. Curves extracted from Bakker, Nyborg and Pacejka (1987) for an unspecified radial tire at the same vehicle speed and normal load are shown for relative comparison. The CRREL predictions are slightly different from the Bakker, Nyborg and Pacejka curves, but this is to be expected, as the tires represented are likely different.

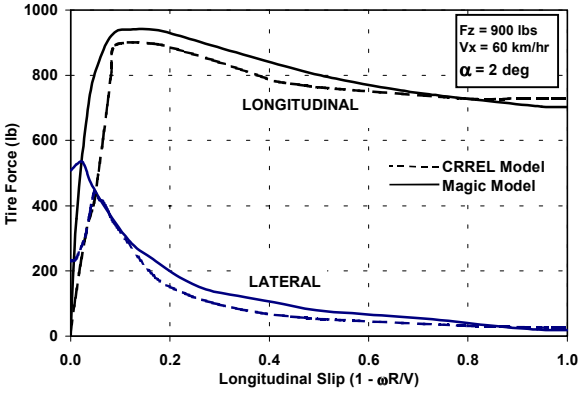

Figure 9: Tire Forces on Dry Pavement - α = 2 deg

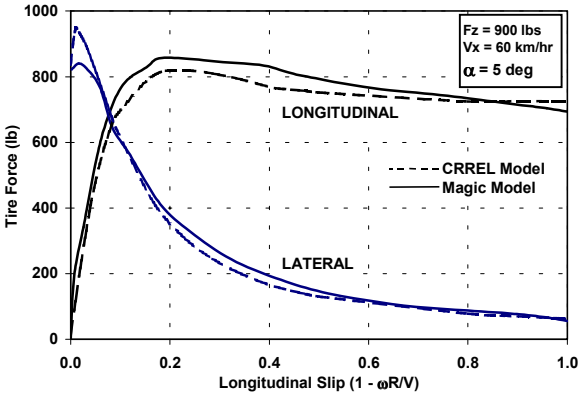

Figure 10: Tire Forces on Dry Pavement - α = 5 deg

Figure 11 shows model predictions of lateral force vs. longitudinal force for different slip angles. The appearance here of dual lateral force values at a single longitudinal force is due to the drop-off in sliding friction with increasing DIV (Figure 4). This behavior is commonly seen in tire test data in the literature, and appears to justify the manner in which the friction coefficient is expressed in the model.

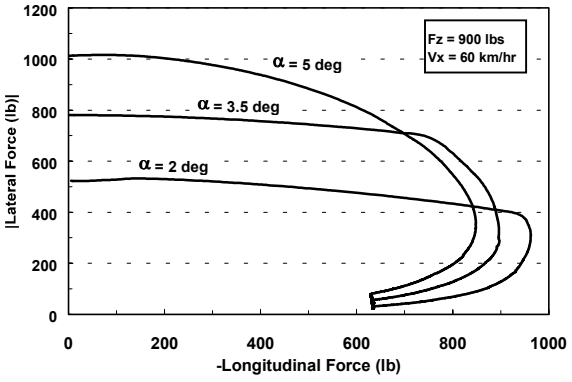

Figure 11: Tire Force Predictions – Dry Pavement

Figure 12 shows lateral force predictions, along with field measurements, for a free rolling tire at different slip angles on compacted snow. (Lateral force (F_y) is non-dimensionalized in this figure by dividing it by the tire vertical force (F_z).) The "snow" curve in Figure 4 is used here to represent the road surface friction coefficient. Model predictions agree very well with measurements.

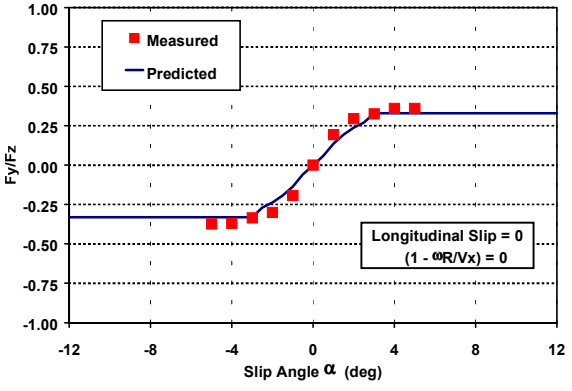

Figure 12: Lateral Force Predictions - Packed Snow

Figures 13 and 14 show sample predictions of Roll moment and Aligning moment on dry pavement. Both are plotted vs. longitudinal force for different slip angles. Test data are not included in these figures for comparison, as it was difficult to obtain accurate representations of these types of measurements.

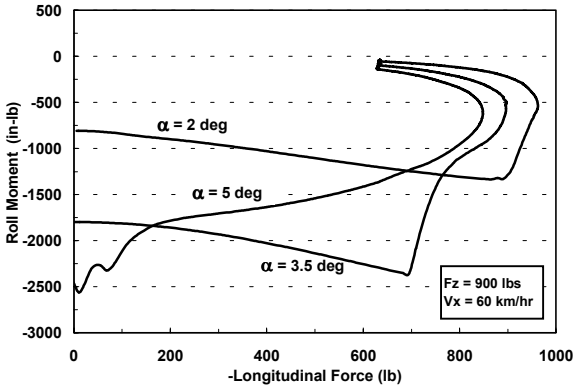

Figure 13: Roll Moment Predictions – Dry Pavement

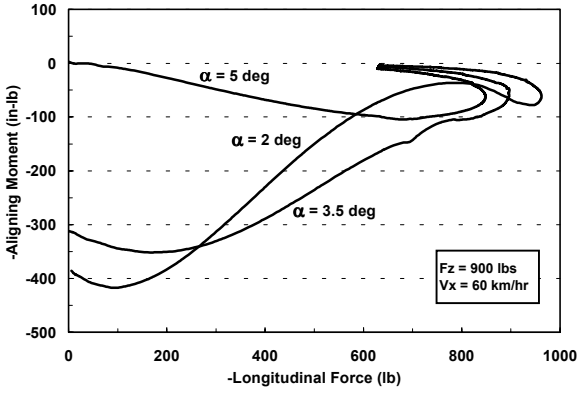

Figure 14: Aligning Moment Predictions – Dry Pavement

ACKNOWLEDGMENTS

This work was supported by the Army ERDC Winter Terrain Effects on Army Simulations Work Package 62784/AT42.

APPENDIX A: DETAILED SOLUTIONS FOR LATERAL TIRE DEFLECTION AND COEFFICIENT "A"

Lateral Deflection "v_x" for $x \le x_m$ (Equation 12)

$$v_x = \frac{Ae^{-\beta(x_m - x)}}{2k\beta}\left(\begin{array}{l}\left(\frac{1}{\beta} + x_m\right)\sin\left(\beta\left(x_m - x\right)\right) \\ \qquad - x_m\left(\beta x_m + 1\right)\cos\left(\beta\left(x_m - x\right)\right)\end{array}\right) + \frac{Ae^{-\beta x}}{2k\beta^2}\sin\left(\beta x\right) + \frac{Ax^2}{k} + \frac{f_{y,sl}e^{\beta x}}{2k\left(x_p - x_m\right)}\left(\begin{array}{l}e^{-\beta x_m}\cos\left(\beta\left(x_m - x\right)\right) \\ \qquad - e^{-\beta x_p}\cos\left(\beta\left(x_p - x\right)\right)\end{array}\right) \quad \text{(A-1)}$$

Lateral Deflection "v_x" for $x > x_m$ (Equation 13)

$$v_x = \frac{Ae^{-\beta(x-x_m)}}{2k}\left(\begin{array}{l}-\left(\frac{1}{\beta^2}\right)\sin(\beta(x-x_m))+x_m^2\cos(\beta(x-x_m))\\ +\frac{x_m}{\beta}(-\cos(\beta(x-x_m))+\sin(\beta(x-x_m)))\end{array}\right)$$
$$+\frac{Ae^{-\beta x}}{2k\beta^2}\sin(\beta x) \qquad \text{(A-2)}$$
$$-\frac{f_{y,sl}}{2k(x_p-x_m)}\left(\begin{array}{l}e^{-\beta(x_p-x)}\cos(\beta(x_p-x))\\ +e^{-\beta(x-x_m)}\cos(\beta(x-x_m))-2\end{array}\right)$$

Coefficient "A" (Equation 15)

$$A=\frac{2k\tan(\alpha)-\frac{f_{y,sl}}{x_m(x_p-x_m)}\varphi_1}{x_m(1+e^{-\beta x_m}\cos(\beta x_m))-\frac{1}{\beta}(1+e^{-\beta x_m}(\sin(\beta x_m)-\cos(\beta x_m)))} \qquad \text{(A-3)}$$

$$\varphi_1 = 1-e^{-\beta(x_p-x_m)}\cos(\beta(x_p-x_m))-e^{-\beta x_m}\cos(\beta x_m)$$
$$+e^{-\beta x_p}\cos(\beta x_p) \qquad \text{(A-4)}$$

APPENDIX B: DETAILED SOLUTIONS FOR ROLL MOMENT AND ALIGNING MOMENT

Roll Moment "M_x" (Equation 23)

$$M_x = \frac{F_z A}{k}\left(\begin{array}{l}\left(\frac{-1}{2\beta^3 x_m}-\frac{1}{2\beta^2}-\frac{x_m}{4\beta}+\frac{1}{4\beta^3 x_p}\right)e^{-\beta x_m}\sin(\beta x_m)\\ +\left(\frac{-1}{2\beta^3 x_m}+\frac{x_m}{4\beta}+\frac{1}{4\beta^3 x_p}\right)e^{-\beta x_m}\cos(\beta x_m)\\ -\frac{1}{4\beta^3 x_p}e^{-\beta x_p}(\sin(\beta x_p)+\cos(\beta x_p))\\ +\left(\frac{-x_m}{2\beta^2 x_p}+\frac{1}{4\beta^3 x_p}+\frac{x_m^2}{4\beta x_p}\right)e^{-\beta(x_p-x_m)}\sin(\beta(x_p-x_m))\\ +\left(\frac{1}{4\beta^3 x_p}-\frac{x_m^2}{4\beta x_p}\right)e^{-\beta(x_p-x_m)}\cos(\beta(x_p-x_m))\\ +\frac{1}{2\beta^3 x_m}-\frac{x_m}{4\beta}+\frac{x_m^2}{3}-\frac{1}{4\beta^3 x_p}+\frac{x_m^2}{4\beta x_p}\\ +\frac{F_z f_{y,sl}}{k(x_p-x_m)}\left(\frac{-\varphi_2}{4\beta x_p}-\frac{1}{\beta x_p}-\frac{x_m}{x_p}+1\right)\end{array}\right)$$

$$\varphi_2 = 3e^{-\beta(x_p-x_m)}(\sin(\beta(x_p-x_m))-\cos(\beta(x_p-x_m))) \qquad \text{(B-1)}$$
$$-e^{\beta(x_p-x_m)}(\sin(\beta(x_p-x_m))+\cos(\beta(x_p-x_m))) \qquad \text{(B-2)}$$

Aligning Moment "M_z" (Equation 25)

$$M_z = Ax_m^3\left(\frac{x_m}{4}-\frac{x_p}{6}\right)+\frac{f_{y,sl}x_m}{2}+C_1\left(1-\frac{V_x}{\omega R}\right)\varphi_3$$
$$+\frac{f_{x,sl}\varphi_4}{x_p-x_m}-\frac{1}{4}A\left(1-\frac{V_x}{\omega R}\right)x_m^4-\frac{f_{x,sl}f_{y,sl}}{C_1(x_p-x_m)} \qquad \text{(B-3)}$$

$$\varphi_3 = \frac{Ax_m^2}{4k\beta^2}e^{-\beta x_m}\sin(\beta x_m)+\frac{Ax_m^4}{4k}$$
$$-\frac{f_{y,sl}x_m}{4k\beta(x_p-x_m)}e^{-\beta x_m}(\sin(\beta x_m)-\cos(\beta x_m))$$
$$-\frac{f_{y,sl}}{4k\beta^2(x_p-x_m)}\left(e^{-\beta x_m}\sin(\beta x_m)-e^{-\beta x_p}\sin(\beta x_p)\right)$$
$$+\frac{f_{y,sl}x_p}{4k\beta(x_p-x_m)}e^{-\beta x_p}(\sin(\beta x_p)-\cos(\beta x_p)) \qquad \text{(B-4)}$$
$$-\frac{f_{y,sl}}{4k\beta}e^{-\beta(x_p-x_m)}(\sin(\beta(x_p-x_m))-\cos(\beta(x_p-x_m)))$$
$$-\frac{f_{y,sl}}{4k\beta^2(x_p-x_m)}e^{-\beta(x_p-x_m)}\sin(\beta(x_p-x_m))$$

$$\varphi_4 = \frac{A(x_m-\frac{1}{\beta})}{4k\beta^2}\left(-e^{-\beta(x_p-x_m)}\left(\begin{array}{l}\sin(\beta(x_p-x_m))\\ +\cos(\beta(x_p-x_m))\end{array}\right)\right)$$
$$+\frac{Ax_m(x_m-\frac{1}{\beta})-\frac{2f_{y,sl}}{x_p-x_m}}{4k\beta}\left(e^{-\beta(x_p-x_m)}\left(\begin{array}{l}\sin(\beta(x_p-x_m))\\ -\cos(\beta(x_p-x_m))\end{array}\right)\right)$$
$$+\frac{A(x_m-\frac{1}{\beta})}{4k\beta^2}+\frac{Ax_m(x_m-\frac{1}{\beta})-\frac{f_{y,sl}}{(x_p-x_m)}}{4k\beta} \qquad \text{(B-5)}$$
$$-\frac{Ae^{-\beta x_p}}{4k\beta^3}(\sin(\beta x_p)+\cos(\beta x_p))+\frac{Ae^{-\beta x_m}}{4k\beta^3}(\sin(\beta x_m)+\cos(\beta x_m))$$
$$+\frac{f_{y,sl}}{k}-\frac{f_{y,sl}}{4k\beta(x_p-x_m)}$$

REFERENCES

Bakker, E., Nyborg, L. and H. B. Pacejka. 1987. Tyre modelling for use in vehicle dynamics studies. SAE Paper #870421. S.A.E. Inc. Warrendale, PA.

Brach, R.M. and R.M. Brach. 2000. Modeling combined braking and steering tire forces. SAE Paper #2000-01-0357. S.A.E. Inc. Warrendale, Pa.

Dixon, J.C. 1996. *Tires, Suspension and Handling*, 2nd ed. S.A.E. Inc. Warrendale, Pa.

Ellis, J.R. 1969. *Vehicle Dynamics*. 20-31. Business Books Limited. London.

Gillespie, T.D. 1992. *Fundamentals of Vehicle Dynamics*, S.A.E. Inc. Warrendale, Pa.

Ichihara, K. 1971. Studies of skidding resistance on road surfaces. *Journal of Research*. p19-20. Public Works Research Institute Ministry of Construction Tokyo, Japan.

Nicolas, V.T. and T.R. Comstock. 1972. Predicting directional behavior of tractor semitrailers when wheel anti-skid brake systems are used. Paper No. 72. ASME Winter Annual Meeting.

Pacejka, H. B. and E. Bakker. 1993. The magic formula tyre model. *Proceedings, 1st Tyre Colloquium, Delft, Oct. 1991*. Supplement to *Vehicle Systems Dynamics*, Vol. 21.

Popov, E.P. 1967. *Introduction to Mechanics of Solids*. p385. Prentice-Hall, Inc. Englewood Cliffs, NJ.

Shim, T., Margolis, D. and C. J. Belltawn. 2000. An Analytical tire model for vehicle simulation in normal driving conditions. SAE Paper #2000-01-0356. S.A.E. Inc. Warrendale, PA.

Shoop, S. A. 1993. Three Approaches to Winter Traction Testing. CRREL Report 93-9. U.S. Army Cold Regions Research and Engineering Laboratory, Hanover. NH.

St. Germann, Wurtenberger, M. and A. Daiβ. 1994. Monitoring of the friction coefficient between tyre and road surface. *IEEE Proceedings of Conference on Control Applications*.

Timoshenko, S. 1960. *Strength of Materials, Part II, Advanced Theory and Problems*. 3rd ed. D. Van Nostrand Co., Inc. Princeton, NJ.

Yamazaki, S., Furukawa, O. and T. Suzuki. 1997. Study on real time estimation of tire to road friction. *Proceedings of the 2nd International Colloquium on Tyre Models for Vehicle Dynamic Analysis*. Supplement to *Vehicle System Dynamics*, 27:225-233. Swets and Zeitlinger Pub. Exton, PA.

AUTHOR BIOGRAPHY

JAMES LACOMBE is a mechanical engineer at CRREL conducting applied research to investigate winter environmental effects on vehicle and tire dynamics, target thermal signatures and infrared sensor performance. His email address is <jlaco@crrel.usace.army.mil>.